P3-31

Progress towards the validation of models of the behavior of neutral helium in gas puff imaging experiments

D.P. Stotler [a,*], J. Boedo [b], B. LeBlanc [a], R.J. Maqueda [c], and S. J. Zweben [a]

[a] *Princeton Plasma Physics Laboratory, Princeton University, P. O. Box 451, Princeton, NJ 08543-0451, USA*

[b] *University of California at San Diego, San Diego, CA, USA*

[c] *Nova Photonics, Los Alamos, NM, USA*

Abstract

Gas puff imaging (GPI) experiments are designed to provide high time and space resolution data on the structure of plasma turbulence in the plane perpendicular to the magnetic field. We first examine the temporal behavior of the helium atoms used as the emitting species for GPI and show that for the time scales of interest ($\gtrsim 1$ μs), the atomic physics model underlying the conventional interpretation of GPI is valid. Second, we continue the Monte Carlo neutral transport simulations of the GPI diagnostic begun in [1]. The radial characteristics of the simulated emission clouds match observations to within the estimated errors. The upshot of these two results is that the technique for unfolding the 2-D, time-dependent plasma density and temperature data from helium GPI emission, relying on this atomic physics model and utilizing DEGAS 2's simulated neutral density data, is valid.

Key words: (PSI-17) Neutral modeling, DEGAS, NSTX, Edge plasma, Collisional-radiative model, (JNM) T0100 Theory and Modeling
PACS: 52.25.Ya, 52.55.Fa, 52.65.Pp, 52.70.Kz

* Corresponding and presenting author
Email address: dstotler@pppl.gov (D.P. Stotler).

1 Introduction

The gas puff imaging (GPI) diagnostic [2,3,4] is designed to provide high time resolution, two-dimensional (2-D) data on plasma turbulence for comparison with three-dimensional (3-D) nonlinear plasma simulation codes, reduced theoretical turbulence models, and direct probe measurements of the turbulence. The technique consists of recording with high temporal and spatial resolution [2] light generated by neutral atoms puffed into the edge of the plasma.

Previous modeling and analysis [3,5] have demonstrated that the behavior of the neutral atoms does not cause the spatial characteristics of the observed emission patterns to deviate qualitatively from those of the underlying plasma turbulence. In Sec. 2, we will examine the impact of the atoms on the temporal characteristics of the GPI diagnostic, using the methods of [6] to show for the time scales of interest that the model behind the conventional interpretation of GPI data is valid. In Sec. 3, we continue the comparison of 3-D, steady state DEGAS 2 [7] neutral transport simulations with GPI observations, begun in [1], using data from 2004 NSTX experiments [4].

2 Time Dependent Response of Helium Atomic Physics Models

2.1 Criteria for Evaluating Collisional Radiative Models

The conventional interpretation of GPI [3] relies on an atomic physics model in which only the atom's ground state is explicitly considered; the effects of all excited states are folded into effective rates for ionization and photon emission. This approach assumes first that this approximate atomic physics model is valid for the parameters of interest and second that the time response of this model for GPI relevant plasma density and temperature changes is accurate. However, these assumptions may not always be true, particularly when metastable states, such as the 2^1S and 2^3S states in helium, are involved. If these assumptions are violated, the temporal *and spatial* characteristics of the observed turbulence could differ from those of the underlying plasma turbulence. A more complex helium atomic physics model requiring the explicit consideration of these metastable states in addition to the ground state is also available [8,9]. The same questions of validity and time response can be asked of this model. Furthermore, one would like to know if the added complexity of this model is offset by a wider range of validity or by

better time resolution.

The full system of equations describing the evolution of the various helium atomic states can be written as [6,8,9,10]

$$\dot{\mathbf{n}} = \mathbf{M}\mathbf{n} + \mathbf{\Gamma}, \tag{1}$$

where $\mathbf{n}$ is a vector of N atomic states, 1^1S, 2^1S, 2^3S, 2^1P, 2^3P, 3^1S, etc., $\mathbf{M}$ is an $N \times N$ matrix of rates, and $\mathbf{\Gamma}$ represents sources of the states. Since the detailed contributions to $\mathbf{M}$ are not referred to further in this paper, we will only note that they consist of the rates for collisional ionization, excitation, de-excitation, radiative decay, and recombination (three body, radiative, and dielectronic). The reader should refer to [9] for additional details on these rates.

The general tactic behind the effective atomic physics models we consider here, referred to as "collisional radiative" (CR) models, [11,12] is to first divide the N states into two sets P and Q (following Greenland's nomenclature [6,10]):

$$\begin{bmatrix} \dot{\mathbf{n}}_P \\ \dot{\mathbf{n}}_Q \end{bmatrix} = \begin{bmatrix} \mathbf{M}_P & \mathbf{H} \\ \mathbf{V} & \mathbf{M}_Q \end{bmatrix} \begin{bmatrix} \mathbf{n}_P \\ \mathbf{n}_Q \end{bmatrix} + \begin{bmatrix} \mathbf{\Gamma}_P \\ \mathbf{\Gamma}_Q \end{bmatrix}, \tag{2}$$

where there are N_P states in the set P and N_Q in Q, with $N = N_P + N_Q$. The traditional approach is to require that the densities of the Q states vary more rapidly than those of the P states [11,12]. However, the key point of Greenland's analysis is that this criterion is insufficient; instead, the P and Q states must be chosen based on the eigenvectors of $\mathbf{M}$.

The key objective of a CR model is to fold the behavior of the Q states into a set of effective rates, $\mathbf{M}_{\text{eff}}$, so that the full system can be described approximately by

$$\dot{\mathbf{n}}_P = \mathbf{M}_{\text{eff}}\mathbf{n}_P + \mathbf{\Gamma}'_P. \tag{3}$$

A set of population coefficients provides the densities of the Q states in terms of the $\mathbf{n}_P$,

$$\mathbf{n}_Q = \mathbf{\Omega}\mathbf{n}_P - \mathbf{M}_Q^{-1}\mathbf{\Gamma}_Q; \tag{4}$$

the expression to be used for $\mathbf{\Omega}$ will be discussed below. Since N_P is typically on the order of a few and much smaller than N (e.g., $N = 59$ for helium [9]), Eq. (3) is vastly preferable to Eq. (1) as the basis for simulating the transport of these species in a code like DEGAS 2 or in interpreting their experimentally observed light emission. The papers by Greenland[6,10] provide specific criteria for assessing the accuracy of Eqs. (3) and (4) as substitutes for Eq. (1). A CR model

(a particular choice of the P and Q states) that fails to meet these criteria is characterized by Greenland as "invalid". For "valid" models, Greenland's analysis also yields the timescales over which this approximate representation is accurate.

These criteria utilize the normalized eigenvectors and eigenvalues of $\mathbf{M}$. The N eigenvectors are used as the columns of an $N \times N$ matrix $\mathbf{T}$, arranged in order of increasing eigenvalue, $\lambda^{(i)}$, $i = 1, \ldots, N$. The resulting matrix is then broken up into four sub-matrices as in Eq. (2),

$$\mathbf{T} = \begin{bmatrix} \mathbf{T}_P & \boldsymbol{\Delta} \\ \boldsymbol{\delta} & \mathbf{T}_Q \end{bmatrix}. \tag{5}$$

In terms of these quantities, $\boldsymbol{\Omega} = \boldsymbol{\delta}\mathbf{T}_P^{-1}$. Greenland shows that in order for a particular CR model to be valid, one must have $\|\boldsymbol{\delta}\| \ll 1$ and $\|\mathbf{T}_Q^{-1}\boldsymbol{\delta}\| \ll 1$ [6]. Furthermore, if the largest P space eigenvalue is much less than the smallest Q space eigenvalue, $|\lambda_P| \ll |\lambda_Q|$, then the usual prescription (e.g., as in [11,12]) for determining $\mathbf{M}_{\text{eff}}$ and $\boldsymbol{\Omega}$ applies [6]; e.g., $\boldsymbol{\Omega} = -\mathbf{M}_Q^{-1}\mathbf{V}$. The time scales corresponding to the inverses of these eigenvalues characterize the time resolution provided by the CR model. In particular, phenomena occurring faster than $\tau_Q \equiv 1/|\lambda_Q|$ are not resolved; i.e., the model treats those time scales as being instantaneous.

2.2 Application to Helium Collisional Radiative Models

Following [8] and [9], we consider two CR models for helium. In Fujimoto's "Formulation I", the P states consist of the ground state 1^1S and the two metastable $n = 2$ states, 2^1S, and 2^3S (we will refer to this model as $N_P = 3$). In "Formulation II", the set P contains just the ground state ($N_P = 1$). We will use two sets of plasma parameters relevant to NSTX GPI experiments [3,4]. One ($T_e = 3$ eV, $n_e = 10^{18}$ m^{-3}) represents the far SOL near the gas manifold; the second ($T_e = 15$ eV, $n_e = 6 \times 10^{18}$ m^{-3}) is characteristic of the center of the emission cloud. We also consider a third, low density set of parameters ($T_e = 30$ eV, $n_e = 10^{16}$ m^{-3}), typical of those used in the original work of Fujimoto [8].

The results of applying the analysis described in [6] and Sec. 2.1 to Goto's CR models [9] are presented in Table 1. The $N_P = 1$ CR model yields $\|\boldsymbol{\delta}\| \ll 1$ and $\|\mathbf{T}_Q^{-1}\boldsymbol{\delta}\| \ll 1$ in all three cases, and is, thus, valid for these plasma conditions, albeit with varying time resolution, τ_Q. The $N_P = 3$ model, however, has small $\|\boldsymbol{\delta}\|$ and $\|\mathbf{T}_Q^{-1}\boldsymbol{\delta}\|$ only in the lowest density case; under these conditions, the $N_P = 3$ model is the more accurate of the two and has much higher time resolution. At higher

(T_e eV, n_e m^{-3}) =	(3, 10^{18})	(15, 6×10^{18})	(30, 10^{16})
Form. I, $N_P = 3$:			
$\|\boldsymbol{\delta}\|$	7.3×10^{-2}	5.4×10^{-1}	1.6×10^{-3}
$\|\mathbf{T}_Q^{-1}\boldsymbol{\delta}\|$	1.1×10^{-1}	6.9×10^{-1}	2.7×10^{-3}
τ_Q (μs)	0.087	0.045	0.52
Form. II, $N_P = 1$:			
$\|\boldsymbol{\delta}\|$	8.2×10^{-5}	2.5×10^{-3}	1.0×10^{-2}
$\|\mathbf{T}_Q^{-1}\boldsymbol{\delta}\|$	8.7×10^{-5}	1.9×10^{-3}	1.0×10^{-2}
τ_Q (μs)	14	0.61	980

Table 1
The results of applying Greenland's validity criteria [6] to the helium collisional radiative models described by [9].

densities, collisional depopulation of the metastable states becomes important, diminishing their lifetime and rendering separate treatment of them less accurate. The 3 eV temperature of the "far SOL" case is low enough to offset the higher density so that the $N_P = 3$ model is marginally valid (in the sense of [6]), but for the "cloud center" conditions, it is not valid at all!

Applying Greenland's algorithm for *choosing* the P and Q states [10] to the GPI relevant density and temperature pairs indicates that an $N_P = 4$ model in which the 2^3P state is added to 1^1S, 2^1S, and 2^3S would be more accurate. However, this model is not valid for the lowest density case. Hence, only the $N_P = 1$ model is valid for all three parameter sets.

To confirm these conclusions and to gain quantitative insight into the time resolution of the CR models, we next consider direct integration of Eqs. (1), (3) and (4). First, we assume an initial 1^1S density of unity and steady plasma parameters. The 3^3D state (upper state for the 587.6 nm line used in the GPI experiments) densities obtained for the GPI relevant density and temperature pairs are depicted in Fig. 1. The τ_Q values from Table 1 are included in Fig. 1 to facilitate comparison with the above analysis.

The validity of the $N_P = 1$ CR model for both plasma parameter sets at times later than τ_Q is confirmed by the convergence of its 3^3D density with that from the full equations. For the $T_e = 3$ eV, $n_e = 10^{18}$ m^{-3} case, the $N_P = 3$ CR model exhibits similar behavior. Under these conditions, the $N_P = 3$ model could be used to obtain higher time resolution than that provided by the $N_P = 1$ CR

model. However, for the "cloud center" parameters, the $N_P = 3$ density differs from that of the full equations for the interval between the two τ_Q values ($0.045 \rightarrow 0.61$ μs); in this sense, the $N_P = 3$ model is invalid.

To further illustrate these results, we again integrate Eqs. (1), (3) and (4), but with n_e and T_e varying in time with a to-be-specified time scale τ so as to resemble a passing turbulent "blob", Fig. 2(a). These integrations begin with a $t_0 = 140$ μs quiescent period at $n_e = 10^{18}$ m^{-3} and $T_e = 3$ eV to permit the 3^3D state to equilibrate with respect to the ground state. Then, n_e and T_e are ramped up to 6×10^{18} m^{-3} and 15 eV, respectively, and back down over a total period of 60τ.

For the $N_P = 1$ model, the 3^3D to ground state density ratio is just a function of n_e and T_e, an element of $\mathbf{\Omega}$ in Eq. (4). That is, this CR model assumes that this density ratio adjusts instantaneously to variations in n_e and T_e and that only the ground state density changes in time when the plasma parameters are constant. Hence, the $N_P = 1$ density ratios for $\tau = 1$ and 0.01 μs match exactly when plotted against the normalized time in Fig. 2(b).

The $\tau = 1$ μs waveform has been designed to be directly relevant to the NSTX GPI experiments; blob autocorrelation times in NSTX are ~ 40 μs [3]. In this case, the density ratios computed with both CR models are very close to those found with the full equations, as one would expect from Fig. 1. Hence, the $N_P = 1$ model will suffice for analyzing these experiments.

The much faster $\tau = 0.01$ μs waveform allows us to estimate the error incurred when a CR model is used on time scales that are shorter than it can handle. Not surprisingly, neither of the CR models accurately matches the density ratio computed from the full equations. However, because the peak density ratios obtained with the two CR models are off by a factor of ~ 2 or less, they might still be useful for qualitative analysis on this time scale.

We conclude that the $N_P = 1$ CR model is valid for the parameters of interest and, at "cloud center" conditions, provides the ≥ 1 μs time resolution needed to match the $\leq 10^6$ frames/s framing rates typically used in GPI experiments [3]. If future GPI cameras are able to resolve shorter timescales, the $N_P = 4$ model described above may be needed to describe the temporal evolution of the helium atoms. As is implied by the $\tau = 1$ μs result of Fig. 2(b), the light emission in the far SOL is negligible so that the $N_P = 1$ model's slower time response there is not relevant.

3 Three-Dimensional Modeling

The 3-D neutral helium density profile in GPI experiments is the result of atoms propagating radially across the scrape-off layer, effectively averaging over the turbulent structures in the plasma, both temporally and spatially, along the way. Consequently, we expect that the neutral density profile computed by a steady state neutral transport simulation will not differ significantly from the actual (i.e., temporally varying) profile. The resulting profile can be used for further analysis of the NSTX GPI camera data (Sec. 4). Furthermore, these relatively straightforward simulations provide an excellent opportunity to validate our model for neutral transport in these experiments, i.e., DEGAS 2; in a sense this also validates the methods used to interpret GPI experimental data.

The 3-D DEGAS 2 simulations of NSTX GPI experiments described here use the $N_P = 1$ CR model for helium [9]. As in [1], these simulations are fully 3-D, including the shape of the gas manifold and emulation of the 64 by 64 pixel fast camera view. The resulting (steady state) 587.6 nm camera images are again compared with the median average [1] over the 300 frames recorded by the GPI camera. We use the median, rather than simple, average so as to minimize the effect of "blobs", yielding an emission cloud representative of the quiescent background plasma. The nonlinearity in the GPI camera response [4] has been fit with a power law function (exponent of 0.475), and the inverse of that function applied to the GPI data so that the resulting quantity is proportional to the number of photons / m^2 s st striking the camera lens.

We consider here NSTX discharges 112811 (H-mode) and 112814 (L-mode). The DEGAS 2 meshes are based on EFIT [13] equilibria at the times of interest. The plasma densities and temperatures are derived from Thomson scattering profiles taken at midplane and are assumed to be constant on a flux surface with $n_i = n_e$ and $T_i = T_e$. For shot 112814, the smoothed Thomson profiles taken at $t = 0.277$ s and 0.293 s have been averaged to approximate the profiles at the time of the GPI observation, $t = 0.285$ s (Fig. 3). Note that since the 1-D Thomson scattering data are inherently incapable of adequately describing a 3-D, turbulent plasma, we can only seek out shots in which the profiles show no obvious effects from passing turbulent structures and then assume that these profiles are representative of the quiescent or average plasma conditions.

The spatial orientation of the camera used in these experiments was absolutely calibrated with a fixed "target plate" and measuring arm before and after the 2004 NSTX run campaign; the uncertainty in these calibrations is ± 1 pixel. The two

calibrations differ by a radial shift of 6 pixels due to a discrete change in the optics. Since we do not know when during the run campaign the change occurred, we cannot be completely sure which of the two calibrations to use with the simulations. We have opted for the pre-run calibration primarily because the post-run calibration places the peaks of the observed emission clouds at locations corresponding to electron temperatures in the 6–8 eV range, well below helium's ionization energy of 24.6 eV. In contrast, the pre-run calibration points to electron temperatures of 15–18 eV at the emission cloud peaks and rising well above the ionization energy on the radially inward half of the clouds where the emission drops off.

The camera images from the resulting simulations are shown in Fig. 4. The color map has been adjusted so that the cyan contour roughly corresponds to half of the peak value. The 25%, 50%, and 75% contours from the median average of the GPI data are overlaid on these images. As indicated by the arrows in Fig. 4, the GPI camera is oriented [4] so that the horizontal axis of its field of view is locally perpendicular to flux surfaces and its vertical axis is aligned with the flux surfaces. The camera's field of view corresponds to a 20 cm by 20 cm square about 20 cm above midplane and roughly centered on the separatrix. The core plasma is to the left of the frame and the gas manifold is at its right edge.

We believe that the vertical variation in the experimental images is dominated by vignetting in the optical system, and we will not compare the vertical characteristics of the simulated and observed images. Instead, we have used a "white plate" image to calibrate the vignetting and have applied this as a filter to the simulated images in Fig. 4.

We now compare the radial characteristics of the images. The locations of the peaks of the simulated and observed emission clouds differ by 2 pixels (the width of one pixel corresponds to a distance of 0.36 cm at the location of the emission cloud). The FWHM of the simulation of the H-mode shot 112811 is 3 pixels narrower than the experimental image (6 pixels vs. 9); the widths for shot 112814 differ by less than 1 pixel.

Considering the uncertainties that enter into this comparison, quantifiable or otherwise, we cannot expect to obtain better agreement than this. First, because both actual and simulated camera images consist of discrete pixels, the radial characteristics of the emission clouds can be made no more precise than one pixel. The finite size of DEGAS 2's mesh "zones" contributes some amount of error to the simulated image characteristics, although care was taken to keep this below one pixel. The ± 1 pixel uncertainty in the spatial calibration of the GPI camera should be taken into consideration in comparing the peak locations; it does not, however,

affect the FWHM.

The uncertainties associated with the error bars in the plasma profiles (Fig. 3) input to DEGAS 2 have been estimated by carrying out 20 variants of the simulation of shot 112811 in which the n_e and T_e profiles have been sampled from within the stated error bars. The resulting distribution of radial peak locations had an average value matching that of the baseline simulation [Fig. 4(a)] and a standard deviation of 1 pixel. The average of the FWHM values was 6.5 pixels, again with a standard deviation of 1 pixel. Passing turbulent structures represent another, more difficult to quantify, source of uncertainty in the Thomson scattering profiles, although the profiles for shot 112811 in Fig. 3 do not appear to be so affected. Likewise, the "median averaging" technique may not be completely eliminating the impact of turbulent structures on the GPI camera images; again, the magnitude of this effect is hard to quantify. Namely, because the relation between the plasma parameters and the light emission is nonlinear, there is no obvious method for incorporating the blobs into these simulations in an average fashion. Instead, they would likely have to be dealt with via time-dependent and 3-D plasma profiles, yielding vastly more complicated simulations.

4 Conclusions

The analysis of Sec. 2 leads us to conclude that the single state atomic physics model conventionally used in the interpretation of helium GPI experiments is valid for the relevant range of plasma parameters and provides adequate time resolution at the cloud center. We are then justified in exploiting the simple relationship between the plasma parameters and the GPI light emission, S, provided by this model: $S = n_0 F(n_e, T_e)$, where F represents the photon emission rate per atom computed from the model. If the neutral density n_0 appearing in this relation can be estimated, the spatial and temporal variation of the electron density and temperature can be unfolded from the GPI images by inverting F (for additional details, see [1,14]). The resulting 2-D and time-varying data can then be used, for example, to test models of blob birth and propagation [14]. The 3-D, steady state DEGAS 2 neutral transport simulations described in Sec. 3 give the neutral density required by this technique. The fidelity of this neutral density profile, and indeed, of the entire model of the helium-based GPI diagnostic, is confirmed by the satisfactory agreement between the simulated and observed emission clouds noted in that section.

Acknowledgments

This work supported by U.S. DOE Contracts DE-AC02-76CHO3073, DE-FG03-95ER54294, and DE-FG02-04ER54520. The authors would like to thank S. A. Sabbagh for generating EFIT equilibria for 112811 on short notice.

References

[1] D. P. Stotler et al., Contrib. Plasma Phys. 44 (2004) 294.

[2] R. J. Maqueda et al., Sci. Instrum. 74 (2002) 2020.

[3] S. J. Zweben et al., Nucl. Fusion 44 (2004) 134.

[4] S. J. Zweben et al., Phys. Plasmas 13 (2006) 056114.

[5] D. P. Stotler et al., J. Nucl. Mater. 313–316 (2003) 1066.

[6] P. T. Greenland, J. Nucl. Mater. 290–293 (2001) 615.

[7] D. P. Stotler, C. F. F. Karney, Contrib. Plasma Phys. 34 (1994) 392.

[8] T. Fujimoto, J. Quant. Spectrosc. Radiat. Transfer 21 (1979) 439.

[9] M. Goto, J. Quant. Spectrosc. Radiat. Transfer 76 (2003) 331.

[10] P. T. Greenland, Proc. R. Soc. Lond. A 457 (2001) 1821.

[11] D. R. Bates et al., Proc. Roy. Soc. Lond. A 267 (1962) 297.

[12] L. C. Johnson, E. Hinnov, J. Quant. Spectrosc. Radiat. Transfer 13 (1973)

[13] L. L. Lao et al., Nucl. Fusion 25 (1985) 1611.

[14] J. R. Myra et al., Phys. Plasmas (in press).

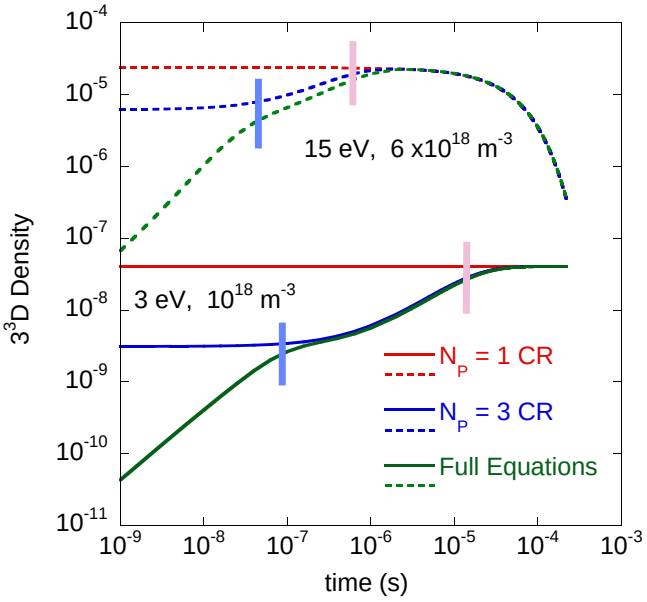

Figure 1. Evolution of the 3^3D density starting with unit ground state density. Three curves are shown for each set of plasma parameters, corresponding to the two collisional radiative models, Eqs. (3) and (4), with $N_P = 1$ and 3, and the full set of equations, Eq. (1). The values of τ_Q from Table 1 are shown as pink (blue) vertical bars for $N_P = 1$ (3).

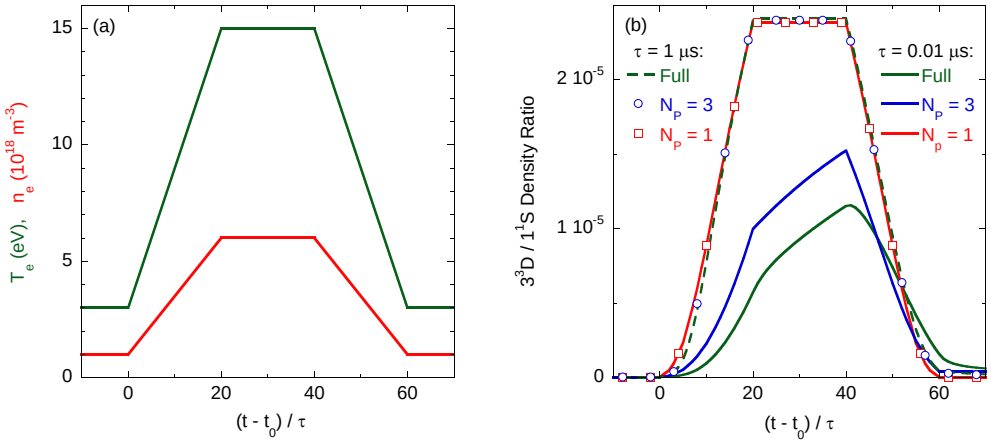

Figure 2. (a) Waveform for n_e and T_e used to represent a passing blob; the parameters are held constant from $t = 0$ through $t_0 = 140$ μs. (b) Resulting variation of the 3^3D to ground state density ratio for the two collisional radiative models and the full set of equations with blob time scales of $\tau = 1$ and 0.01 μs.

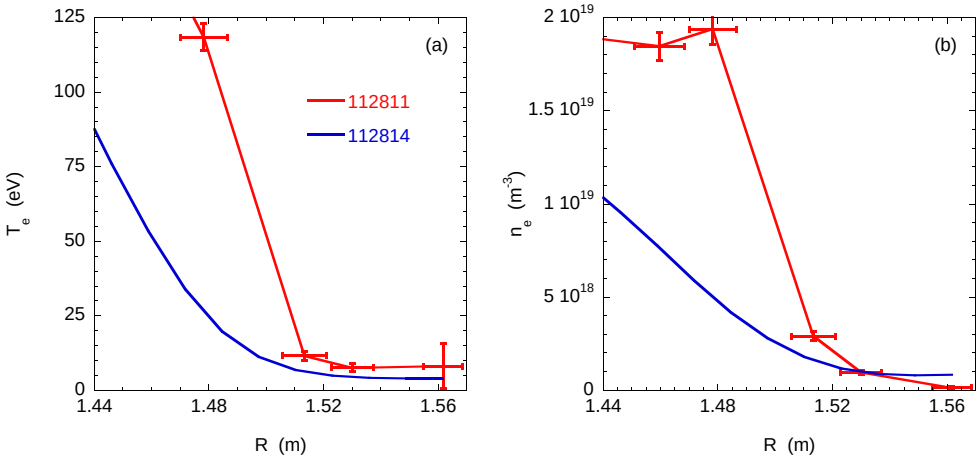

Figure 3. Thomson scattering electron temperature (a) and density (b) profiles used in DEGAS 2 simulations of shots 112811 and 112814. Since the data from 112811 are used directly, the associated error bars are also plotted. The profiles for 112814 are the average of the smoothed Thomson scattering (TS) profiles for time slices before and after the GPI time.

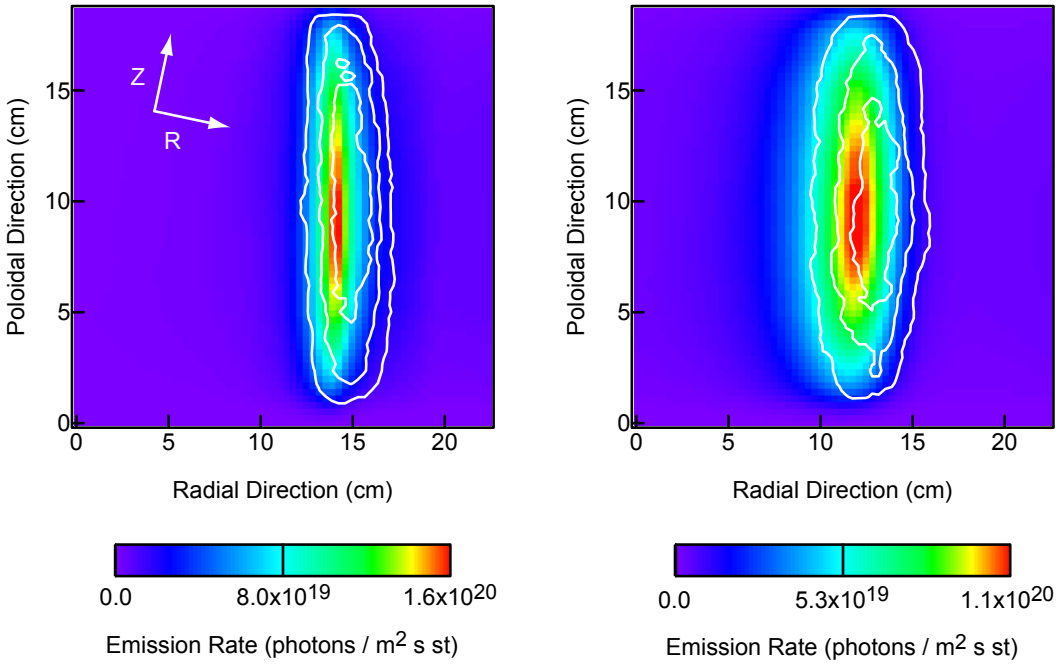

(a) (b)

Figure 4. Simulated (color images) and observed (line contours) camera data for NSTX shots 112811 (a) and 112814 (b). The experimental data are not absolutely calibrated. The simulations assume an experimentally relevant source rate of 6×10^{20} atoms / s [3]. The arrows in (a) indicate the directions of increasing major radius R and height above midplane Z.